Monthly Notices of the ROYAL ASTRONOMICAL SOCIETY

MNRAS **501,** 5723–5732 (2021) doi:10.1093/mnras/staa4048
Advance Access publication 2021 January 7

A numerical jet model for the prompt emission of gamma-ray bursts

Ruben Farinelli [1]★ Rupal Basak,[1,2] Lorenzo Amati,[1] Cristiano Guidorzi[1,2,3] and Filippo Frontera[2]

[1]*INAF – Osservatorio di Astrofisica e Scienza dello Spazio di Bologna, Via P. Gobetti 101, I-40129 Bologna, Italy*
[2]*Dipartimento di Fisica e Scienze della Terra, Università di Ferrara, Via Saragat 1, I-44122 Ferrara, Italy*
[3]*INFN – Sezione di Ferrara, Via Saragat 1, I-44122 Ferrara, Italy*

Accepted 2020 December 22. Received 2020 December 22; in original form 2020 October 22

ABSTRACT

Gamma-ray bursts (GRBs) are known to be highly collimated events, and are mostly detectable when they are seen on-axis or very nearly on-axis. However, GRBs can be seen from off-axis angles, and the recent detection of a short GRB associated with a gravitational wave event has conclusively shown such a scenario. The observer viewing angle plays an important role in the observable spectral shape and the energetic of such events. We present a numerical model that is based on the single-pulse approximation with emission from a top-hat jet and has been developed to investigate the effects of the observer viewing angle. We assume a conical jet parametrized by a radius $R_{\rm jet}$, half-opening angle $\theta_{\rm jet}$, a comoving-frame emissivity law and an observer viewing angle $\theta_{\rm obs}$, and then study the effects for the conditions $\theta_{\rm obs} < \theta_{\rm jet}$ and $\theta_{\rm obs} > \theta_{\rm jet}$. We present results considering a smoothly broken power-law emissivity law in jet comoving frame, albeit the model implementation easily allows to consider other emissivity laws. We find that the relation $E^{\rm i}_{\rm p} \propto E^{0.5}_{\rm iso}$ (Amati relation) is naturally obtained from pure relativistic kinematic when $\Gamma \gtrsim 10$ and $\theta_{\rm obs} < \theta_{\rm jet}$; on the contrary, when $\theta_{\rm obs} > \theta_{\rm jet}$ it results $E^{\rm i}_{\rm p} \propto E^{0.25}_{\rm iso}$. Using data from literature for a class of well-know sub-energetic GRBs, we show that their position in the $E^{\rm i}_{\rm p}$–$E_{\rm iso}$ plane is consistent with event observed off-axis. The presented model is developed as a module to be integrated in spectral fitting software package XSPEC and can be used by the scientific community.

Key words: radiation mechanisms: non-thermal – methods: numerical – software: simulations – gamma-ray burst: general.

1 INTRODUCTION

Gamma-ray bursts (GRB) remain one of the most debated transient phenomena even after decades of research. It is fairly established that a GRB is a highly collimated event powered by a relativistic jet (Sari, Piran & Halpern 1999; Aloy et al. 2000; Zhang, Woosley & MacFadyen 2003), launched during the catastrophic death of a massive star (Woosley 1993) or a coalescence event between two neutron stars or a neutron star – black hole pair (Eichler et al. 1989; Li & Paczyński 1998; Abbott et al. 2017a). The radiation process of the prompt emission phase remains at the centre of the debate ever since their discovery. From theoretical considerations, synchrotron emission in an ordered or random magnetic field seems to be a good description of the broad-band spectra (Meszaros & Rees 1993; Katz 1994; Meszaros, Rees & Papathanassiou 1994; Ghisellini & Lazzati 1999). But, based on the spectral index below the peak energy and the efficiency of gamma-ray photon production, the models involving synchrotron process face some criticism (Crider et al. 1997; Preece et al. 1998; Kaneko et al. 2006, though see Burgess et al. 2019). Several alternative models have been proposed like synchrotron self-Compton (Dermer, Chiang & Mitman 2000; Nakar, Ando & Sari 2009), inverse-Compton scattering (Lazzati et al. 2000; Barniol Duran, Bošnjak & Kumar 2012), different flavours of photospheric models (Beloborodov 2011; Lundman, Pe'er & Ryde 2013; Bégué & Pe'er 2015; Ahlgren et al. 2019), as well as hybrid models in which different processes can also evolve in terms of their dominance (Zhang et al. 2018). Usually the prompt GRB spectra are fitted with phenomenological models, such as cut-off power law or the widely used Band function (Band et al. 1993). An additional photospheric component has been sometimes detected and modelled with a blackbody (Ryde et al. 2010). In addition, there have been some recent developments to employ more physically motivated models for the spectral fitting (Burgess et al. 2019). The first physical model (GRBCOMP also released for the XSPEC package) applied to the GRB spectral analysis has been developed by Titarchuk et al. (2012) and later tested on a sample of time-resolved spectra by Frontera et al. (2013).

The spectral models, whether empirical or driven by a physical scenario, mostly have an implicit assumption that the radiation received by the observer comes directly on-axis from the GRB jet (Proga et al. 2003). Due to the relativistic effects the jet is highly collimated and the radiation is indeed beamed within a very narrow cone, which justifies the assumption. However, it is highly probable to see a GRB from an off-axis angle, not necessarily outside the cone, and in general it can potentially alter the observables from an axisymmetric case (e.g. Yamazaki, Ioka & Nakamura 2003; Kathirgamaraju, Barniol Duran & Giannios 2018). The observer viewing angle ($\theta_{\rm obs}$) thus becomes an important parameter in the analysis of the observed light curves and spectra.

Naturally, the relatively nearby GRBs are the most interesting cases of highly off-axis GRBs. For instance, Salafia et al. (2016)

★ E-mail: ruben.farinelli@inaf.it

© 2021 The Author(s)
Published by Oxford University Press on behalf of Royal Astronomical Society

Downloaded from https://academic.oup.com/mnras/article/501/4/5723/6067371 by universita di catania fac giurisprudenza emeroteca user on 13 December 2023

calculated that a sizable fraction, anywhere between 10 per cent to 80 per cent of nearby GRBs (redshift, $z < 0.1$) are detectable from an off-axis angle outside the jet cone by the *Neil Gehrels Swift Observatory* (Gehrels et al. 2004). The recent discovery of a short GRB associated with a gravitational wave signal (GW 170817) has conclusively shown that the GRB was seen from an off-axis angle (Margutti et al. 2017; Abbott et al. 2017a, b).

Another example is GRB 150101B ($z = 0.13$) which may have been seen from an off-axis angle of 13° (Troja et al. 2018) while having a half-opening angle close to 9° (Fong et al. 2016). The nearby low luminosity long GRB sample is also interesting as being faint and nearby there is a good probability that they may fall in the category of GRBs seen off-axis (Fynbo et al. 2004). However, several studies based on radio observation as well as the luminosity function and local rate have suggested that they might be intrinsically fainter rather than being seen off-axis, and can even belong to a different population compared to the cosmological high-luminosity GRB class (Soderberg et al. 2004, 2006; Pian et al. 2006; Liang et al. 2007). On the other hand, hydrodynamic simulations of GRB jets show that the jet break signature of the off-axis GRBs can be delayed by several weeks and may remain hidden in the data (van Eerten, Zhang & MacFadyen 2010). The lack of jet break signature in *Swift* sample is indeed consistent, and thus provides room for the alternative scenario.

Some of the low-luminosity GRBs are found to be outliers of the Amati relation (Amati et al. 2002, 2006), hereafter AR, which is a relation between the intrinsic peak energy of the $EF(E)$ spectrum ($E_{\rm p}^{\rm i}$) and the isotropically equivalent total emitted energy ($E_{\rm iso}$). They are GRB 980425, GRB 031203, GRB 080517, GRB 100316D, and GRB 171205A (Campana et al. 2006; Ghisellini et al. 2006; Amati et al. 2007; Liang et al. 2007; Starling et al. 2011; Heussaff, Atteia & Zolnierowski 2013; Stanway et al. 2015; D'Elia et al. 2018).

Several studies have been performed to investigate the observational effects of an off-axis jet (e.g. Yamazaki et al. 2003; Guidorzi et al. 2009; Kathirgamaraju et al. 2018), albeit the principally focused on the light-curve shape and temporal variability.

The main goal of this work is to provide to the scientific community the first relativistic jet model for the X-ray spectral fitting package XSPEC (Arnaud 1996). The intrinsic complexity of the jet physics (Mészáros & Rees 2001; Ramirez-Ruiz, Celotti & Rees 2002; Zhang et al. 2003; Zhang, Woosley & Heger 2004; Morsony, Lazzati & Begelman 2007; Mizuta, Nagataki & Aoi 2011) and the need to achieve a trade-off between computational speed and model accuracy leads to introduce unavoidable simplifications in code development. We have built a model based on the so-called single pulse approximation (SPA), where a top-hat relativistic jet instantaneously emits a flash of radiation in the star frame (Yamazaki et al. 2003).

The jet can be viewed at any angle and we obtain the total spectra by integrating over the different areas on the emitting surface. We allow to consider different emissivity laws in the comoving frame. This is thus not a radiative-transfer model, but it parametrizes the geometry of the emission in terms of jet radius and opening angle as well as observer's viewing angle.

In addition to a simple top-hat jet, various theoretical arguments and hydrodynamic simulations, as well as observations, have proposed GRB jets with angular structure (Berger et al. 2003; Basak & Rao 2015; Margutti et al. 2017; Beniamini & Nakar 2019; Salafia et al. 2020), i.e. non-constant Γ-factor. We then also consider the possibility of a structured jet and present some results, albeit in the release for the XSPEC package we implemented the case of a constant Γ-factor, to avoid having a too-high number of free-parameters.

The paper is structured as follows: in Section 2, we present the mathematical formulation of the model. In Section 3, we report results as a function of the input parameters and compare the case of constant and variable Γ factor. In Section 4, we show the important consequences at observational level between on-axis and off-axis cases in terms of the well-known $E_{\rm p}^{\rm i}$–$L_{\rm iso}$ or $E_{\rm p}^{\rm i}$–$E_{\rm iso}$ relations. The discussion and conclusions are presented in Sections 5 and 6, respectively.

2 GEOMETRIC AND PHYSICAL DEFINITION OF THE JET MODEL

2.1 Emission spectra

We present here the mathematical details on which the jet geometry and emission are based. The most important parameters for the problem formulation are shown in Fig. 1. Let us first consider a reference system *XYZ* where the jet axis is aligned with the *Z*-axis. Applying a rotation of an angle $\theta_{\rm obs}$ around the *X*-axis, the top-hat Cartesian coordinates in a system *xyz* where the *z*-axis is directed towards the observer are

$$\begin{aligned} x &= R_{\rm jet}\sin\theta\cos\phi, \\ y &= R_{\rm jet}(\cos\theta\sin\theta_{\rm obs} + \cos\theta_{\rm obs}\sin\theta\sin\phi), \\ z &= R_{\rm jet}(\sin\theta\cos\theta_{\rm obs} - \sin\theta_{\rm obs}\sin\theta\sin\phi), \end{aligned} \tag{1}$$

where $\theta \in [0, \theta_{\rm jet}]$ and $\phi \in [0, 2\pi]$, with $\theta_{\rm jet}$ defined as the jet half-opening angle. The distance of a point *P* on the top-hat surface to the observer located at position *O* with coordinates (0,0,*d*) is

$$r = \sqrt{d^2 - 2R_{\rm jet}\cos\theta_{\rm obs}\cos\theta + 2R_{\rm jet}d\sin\theta_{\rm obs}\sin\theta\sin\phi + R_{\rm jet}^2}. \tag{2}$$

The cosine of the angle between the radial velocity vector and the line from *P* to the observer (*PO*) is

$$\cos\alpha = \frac{-R_{\rm jet} + d\ \cos\theta_{\rm obs}\cos\theta - d\ \sin\theta_{\rm obs}\sin\theta\ \sin\phi}{\sqrt{d^2 + R_{\rm jet}^2 - 2dR_{\rm jet}\cos\theta_{\rm obs}\cos\theta + 2d\ R_{\rm jet}\sin\theta_{\rm obs}\sin\theta\ \sin\phi}}, \tag{3}$$

which becomes for $r << d$

$$\cos\alpha \approx \cos\theta_{\rm obs}\ \cos\theta - \sin\theta_{\rm obs}\ \sin\theta\ \sin\phi. \tag{4}$$

The cosine of the angle formed by *PO* and the *z*-axis is

$$\cos\omega = \frac{1}{r}\left(d - R_{\rm jet}\cos\theta_{\rm obs}\cos\theta + r\sin\theta_{\rm obs}\sin\theta\sin\phi\right), \tag{5}$$

and is ≈1 under the same condition.

The specific intensity in the observer frame is obtained by a Lorentz transformation along with the cosmological correction term and is given by

$$\mathrm{I_{jet}}(\mathbf{k}_{\rm obs}, \mathrm{E_{obs}}) = \frac{\mathrm{I_{jet}}(\mathbf{k}_{\rm jet}, \mathrm{E_{jet}})\mathrm{D_f^3}}{(1+\mathrm{z})^3}, \tag{6}$$

where

$$E_{\rm jet} = \frac{(1+z)E_{\rm obs}}{D_{\rm f}}, \tag{7}$$

while

$$D_{\rm f} = 1/\,\Gamma(1 - \beta\cos\alpha), \tag{8}$$

is the usual Doppler factor, Γ is the bulk Lorentz factor, and β is the fluid's velocity in units of the speed of light. We consider isotropic emissivity in the jet comoving frame so that $I_{\rm jet}(\mathbf{k}_{\rm jet}, E_{\rm jet}) = I_{\rm jet}(E_{\rm jet})$.

Let us now consider an element area on the jet-surface $dA = R_{\rm jet}^2 {\rm d}u\ {\rm d}\phi$, centred at coordinates $[u, \phi]$, where $u = \cos(\theta)$. The

Downloaded from https://academic.oup.com/mnras/article/501/4/5723/6067371 by universita di catania fac giurisprudenza emeroteca user on 13 December 2023

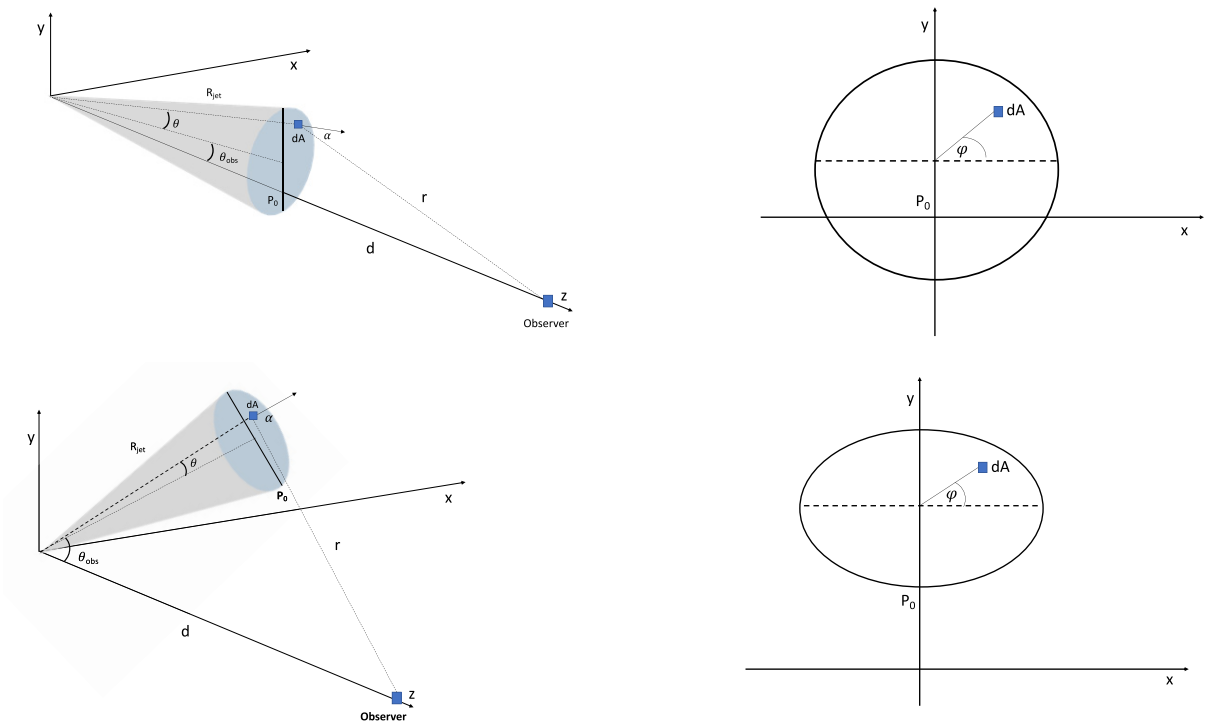

Figure 1. Schematic view of the jet geometry for the on-axis (top-figures) and off-axis (bottom-figures) cases in a reference system xyz where the z-axis is aligned towards the observer. For computing the spectrum (see equation 13) it is more convenient to define the polar and azimuthal angles θ and ϕ in a reference system XYZ rotated by an angle $\theta_{\rm obs}$ around the x-axis and where the Z-axis is aligned with the jet axis. The point P_0 represents the region on the jet surface from where photons first reach the observer.

effective solid angle subtended by this element area is

$$d\Omega_{\rm i,j}^{\rm eff} = (1+z)^4 \frac{R_{\rm jet}^2 \cos\alpha}{D_{\rm L}^2} {\rm d}u\ {\rm d}\phi, \tag{9}$$

where we used the relation $D_{\rm L} = (1+z)^2 D_{\rm A}$ between the angular diameter distance and the luminosity distance, while the term $\cos\alpha$ accounts for the effective projected area.

Combining equations (6) and (9), the flux received by the observer at O from the surface area dA is

$${\rm d}F(E_{\rm obs}) = \frac{(1+z)\ R_{\rm jet}^2}{D_{\rm L}^2} I_{\rm jet}(E_{\rm jet}) D_{\rm f}^3\ \cos\alpha\ {\rm d}u\ {\rm d}\phi. \tag{10}$$

The jet is assumed to emit a single pulse in the stationary (redshift corrected) rest frame so that $L(t_*) = \delta(t_* - t_{*,0})$: because of the curvature effect, the pulse signal duration in the observer frame for $\theta_{\rm obs} \leq \theta_{\rm jet}$ is

$$t_{\rm p}^{\rm on} = (1+z)\frac{R_{\rm jet}}{c}[1 - \cos(\theta_{\rm obs} + \theta_{\rm jet})], \tag{11}$$

while for $\theta_{\rm obs} > \theta_{\rm jet}$ it is

$$t_{\rm p}^{\rm off} = (1+z)\frac{2R_{\rm jet}}{c}\sin\theta_{\rm obs}\sin\theta_{\rm jet}. \tag{12}$$

In the remainder of the paper, we will label as on-axis and off-axis the events belonging to the first and second case, respectively.[1]

[1]Note that some authors label as off-axis the events for which $\theta_{\rm obs} > 0^\circ$, no matter on the value of $\theta_{\rm jet}$.

The flux from the whole top-hat surface averaged over the pulse time $t_{\rm p}$ is obtained as

$$F(E_{\rm obs}) = \frac{(1+z)\ R_{\rm jet}^2}{D_{\rm L}^2\ (t_{\rm p}/{\rm s})} \int_0^{2\pi}\int_{u_{\rm c}}^1 I_{\rm jet}(E_{\rm jet}) D_{\rm f}^3 \cos\alpha\ {\rm d}u\ {\rm d}\phi, \tag{13}$$

with $u_{\rm c} = \cos\theta_{\rm jet}$.

The isotropic equivalent luminosity is computed with the relation

$$L_{\rm iso} = 4\pi D_{\rm L}^2 (1+z) \int_{E_1/(1+z)}^{E_2/(1+z)} F[(1+z)E_{\rm obs}]{\rm d}E_{\rm obs}, \tag{14}$$

and the fluence as

$$E_{\rm iso} = \frac{\Delta t_{\rm obs}}{(1+z)} L_{\rm iso}. \tag{15}$$

The code modularity allows to choose among different models for the emissivity in the comoving frame; we consider first a smoothly broken power law (SBPL) in the form

$$I(E) = K \left(\frac{E}{E_0}\right)^{-p_1} \left\{\frac{1}{2}\left[1 + \left(\frac{E}{E_0}\right)^{1/\delta}\right]\right\}^{(p_1-p_2)/\delta}, \tag{16}$$

with K in units of erg cm^{-2} s^{-1} keV^{-1} ster^{-1} and the parameter δ determines the smoothness of the transitions between the two PL regimes with index p_1 and p_2, and the change of slope occurs in the energy interval $E_1 - E_2$ such that

$$\log_{10}\frac{E_2}{E_0} = \log_{10}\frac{E_0}{E_1} \sim \delta. \tag{17}$$

The second model is a cut-off power law (CPL) defined as

$$I(E) = K(E/{\rm keV})^{-q} {\rm e}^{-E/E_{\rm cut}}. \tag{18}$$

Downloaded from https://academic.oup.com/mnras/article/501/4/5723/6067371 by universita di catania fac giurisprudenza emeroteca user on 13 December 2023

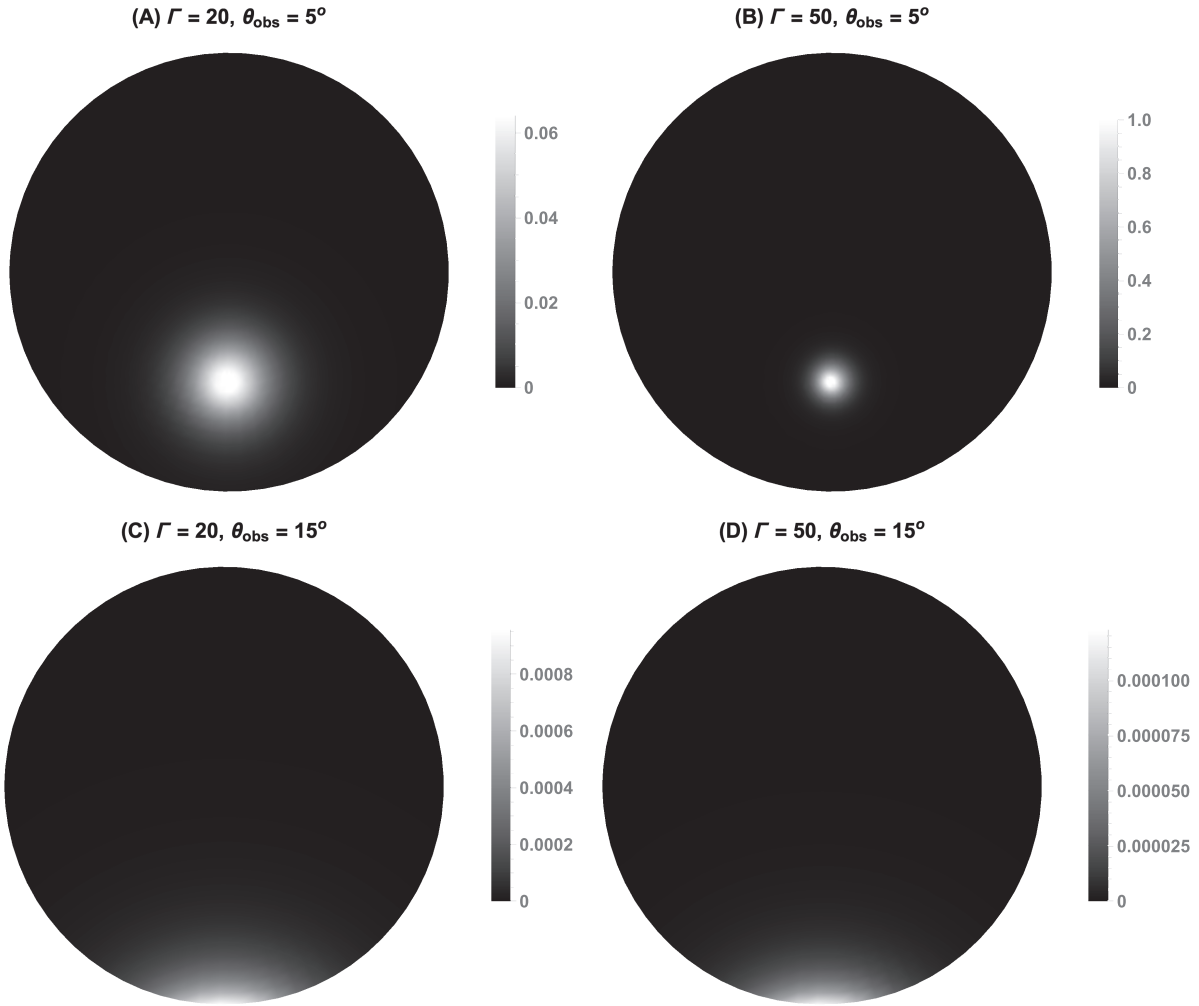

Figure 2. Top-surface brightness along the *xy*-plane of a jet with opening angle $\theta_{\rm jet} = 10^{\circ}$ and different values of the Γ factor and observer's viewing angle. Top-left: (A) $\Gamma = 20$, $\theta_{\rm obs} = 5^{\circ}$, Top-right: (B) $\Gamma = 50$, $\theta_{\rm obs} = 5^{\circ}$, Bottom-left: (C) $\Gamma = 20$, $\theta_{\rm obs} = 15^{\circ}$, Bottom-right: (D) $\Gamma = 50$, $\theta_{\rm obs} = 15^{\circ}$.

Finally, for a thermal component we use a simple blackbody (BB) function

$$I(E) = K \frac{(E/\mathrm{keV})^3}{\mathrm{e}^{E/kT_{\rm bb}} - 1}. \quad (19)$$

The normalization K is allowed to be free in the case of BPL and CPL models, while in the BB case it is dictated by its thermodynamical limit value 5×10^{22} erg cm^{-2} s^{-1} keV^{-1} ster^{-1}. In this paper, all presented results have been obtained assuming a comoving-frame SBPL spectrum.

3 RESULTS

3.1 Constant Γ-factor

In order to emphasize the importance of the observer viewing angle, we show in Fig. 2 the observed surface brightness of the jet for four different combination of $\Gamma = 20$, 50 and $\theta_{\rm obs} = 5^{\circ}$, 15°, while we fix $\theta_{\rm jet} = 10^{\circ}$. The values shown in the colour bars are not in absolute units, but should be used to compare the relative brightness between different cases. The relative brightness drops by several orders of magnitude from a viewing angle inside the jet cone ($\theta_{\rm obs} < \theta_{\rm jet}$, upper panels) to outside the jet cone ($\theta_{\rm obs} > \theta_{\rm jet}$, lower panels). For the former case, i.e. $\theta_{\rm jet} < \theta_{\rm obs}$, the lateral spreading becomes higher and the relative brightness becomes lower as Γ decreases (compare panel A with panel B). However, for $\theta_{\rm jet} > \theta_{\rm obs}$ (see the lower panels), we note an opposite trend. Here, the brightness is relatively higher by a factor of $\sim$8 for lower Γ (compare panel C with panel D). It is evident that we cannot always associate brighter GRBs with higher Γ. The observer needs to be within the jet cone for that to happen, otherwise a reverse variation will be seen.

We then consider the observed spectra and first focus on the cases for different values of the Γ factor for both the on-axis and off-axis case. The results are shown in Fig. 3. The simulations have been performed assuming a jet with $\theta_{\rm jet} = 10^{\circ}$ and radius $R_{\rm jet} = 10^{12}$ cm, and an SBPL emissivity law in the comoving frame with $p1 = 0$, $p2 = 1.5$, $E_0 = 10$ keV, and $\delta = 0.2$.

For the cases $\theta_{\rm obs} < \theta_{\rm jet}$, the spectral peak and flux are positively correlated with the Γ. On the contrary, for observer's viewing angle outside the cone ($\theta_{\rm obs} > \theta_{\rm jet}$), a reverse variation is noticed. It is also worth pointing the significant drop in the received flux for off-axis events, confirming that most of GRBs belonging to this class are likely below the threshold sensitivity of current instruments, unless either the Γ factor is low or they are neighbour (see Section 4).

Downloaded from https://academic.oup.com/mnras/article/501/4/5723/6067371 by universita di catania fac giurisprudenza emeroteca user on 13 December 2023

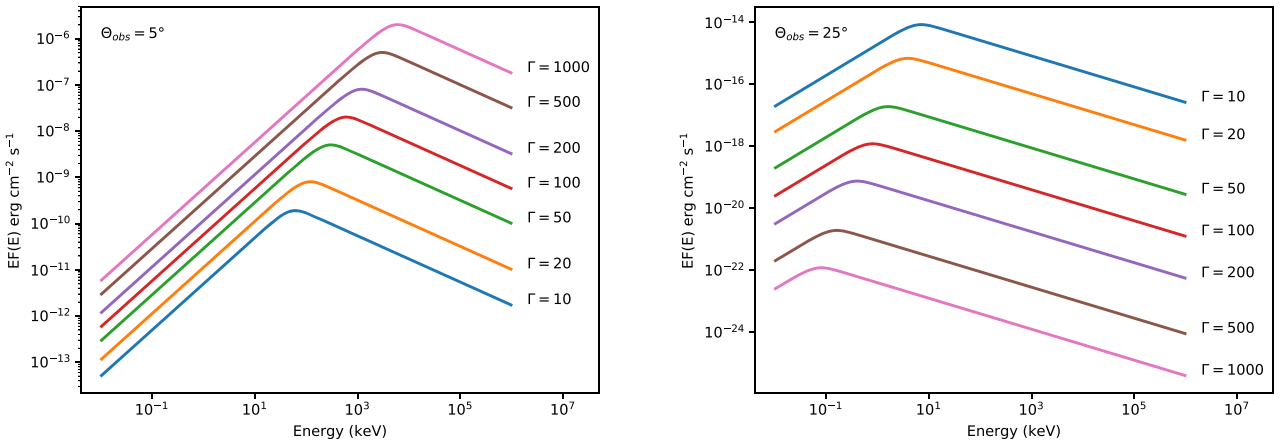

Figure 3. Simulated spectra with Γ varied in the range 10–1000 for a jet with $\theta_{\rm jet} = 10^\circ$, $R_{\rm jet} = 10^{12}$ cm, and a SBPL emissivity law in the comoving frame with $E_0 = 10$ keV, $p_1 = 0$, $p_2 = 1.5$, and $\delta = 0.2$. The two cases for $\theta_{\rm obs} = 5^\circ$ (on-axis) and $\theta_{\rm obs} = 25^\circ$ (off-axis) are reported.

The second parameter we investigated is the jet opening angle $\theta_{\rm jet}$, and results are presented in Fig. 4: for $\theta_{\rm obs} < \theta_{\rm jet}$ and Γ such that $\theta_{\rm jet} > > 1/\Gamma$, all the spectra are equivalent, with their normalization rescaled by the pulse duration $t_{\rm p}$ (see equations 11 and 13). Note that this renormalization unavoidably comes from the model definition, but actually the bulk of the flux comes from a region of angle $\theta \sim 1/\Gamma < < \theta_{\rm jet}$ centred towards the observer's viewing angle, which is independent on $\theta_{\rm jet}$. This can be seen noticing that the observed peak energy $E_{\rm p}$ remains unchanged, and confirms the well-known result that for $\theta_{\rm jet} > 1/\Gamma$ a radially symmetric jet is indistinguishable from an expanding sphere (e.g. Rhoads 1997; Salafia et al. 2016).

Typical GRB Lorentz factors are $\Gamma \gtrsim 100$ (Mészáros 2006), and the effect of observer's viewing angle in the on-axis case would require very collimated jet opening angles $\theta_{\rm jet} \lesssim 1^\circ$. This leads in turn to two consequences at the observational level; first, such very narrow jets (if present) have a very low probability of detection, secondly, the dynamical range of observer's viewing angle with $\theta_{\rm obs} \leq \theta_{\rm jet}$ would be so narrow to essentially suppress any detectable effect.

Nevertheless, for illustrative purposes we report in Fig. 4 (top-left panel) the case of a moderate Lorentz factor $\Gamma = 20$ and values of $\theta_{\rm jet} \lesssim 1/\Gamma$ for a fully on-axis observer ($\theta_{\rm obs} = 0^\circ$). Here, there is not just a simple spectral rescaling due to $t_{\rm p}$ but also a progressive decreases of $E_{\rm p}$ as $\theta_{\rm jet}$ increases. The situation changes when looking outside the jet cone no matter whether $\theta_{\rm jet}$ is lower or higher than $1/\Gamma$: in Fig. 4 (bottom panels) we report simulated spectra again for $\theta_{\rm jet} < 1/\Gamma$ and $\theta_{\rm jet} > > 1/\Gamma$. In this case, the trend is always the same, with $E_{\rm p}$ increasing as $\theta_{\rm jet}$ does as well. This is understood because for off-axis events, the dominant contribution to the observed flux always comes from the region around the bottom border of the jet (see also Fig. 2). For fixed observer's viewing angle, as $\theta_{\rm jet}$ increases the Doppler factor from this area increases, leading in turn of higher observed values of $E^{\rm p}_{\rm obs}$. We also claim that using only spectral fitting, the jet opening angle cannot be measured in the GRB prompt phase for on-axis events apart for the unlikely case $\theta_{\rm jet} \lesssim 1^\circ$ (see top-left panel of Fig. 3), while in principle it could be done for off-axis events (if detectable) where the effect of $\theta_{\rm jet}$ in the observed spectra is much more enhanced. Note that we do not present results for varying values of $R_{\rm jet}$ as the pulse-average flux simply rescales linearly with it (equation 13). Concerning the parameters of the comoving-frame SBPL (equation 16), apart for the low-energy and high-energy slopes (depending on p_1 and p_2, respectively) and the smoothness of the transition at the peak energy E_0 (depending on δ), we point out that the both the flux and $E_{\rm p}$ linearly scales with E_0, for fixed values of $\theta_{\rm obs}$ and jet parameters.

3.2 Structured jet with variable Γ-factor

In a more complicated scenario, the GRB jet may have an angular dependence $\Gamma(\theta)$ of the bulk Lorentz factor (see references in Section 1). Numerical hydrodynamic simulations have been performed for example by Zhang et al. (2003), who showed angular variation of density, flux, and Γ. Later, Lundman et al. (2013, hereafter L13) used an empirical form to characterize the derived Γ-profile. In this section, we explore the effects of a non-constant Γ on the observed properties of our model. In particular, we adopt the analytical function proposed by L13, with slight modification, where we explicitly write the dependence of Γ on θ

$$\Gamma = \Gamma_{\rm min} + \frac{\Gamma_{\rm max} - \Gamma_{\rm min}}{\sqrt{(\theta/\theta_{\rm jet})^{2p} + 1}}, \tag{20}$$

where $\Gamma_{\rm max}$ is the maximum value of the Lorentz factor at the centre of the jet. It is important to keep in mind that $\Gamma_{\rm min}$ *is not* the value of Γ for $\theta = \theta_{\rm jet}$, but it represents an asymptotic value of Γ at the outer layer, for instance in the presence of a sub-relativistic surrounding cocoon. To better show this effect, in Fig. 5, we report the behaviour Γ as a function of θ for the case $\Gamma_{\rm max} = 100$, $\Gamma_{\rm min} = 2$ and two different values of the index p.

To investigate the observational effects of the Γ-stratification, we show in Fig. 6 the observed $E_{\rm p}$ and flux for different values of the observer's viewing angle, with $\theta_{\rm jet} = 10^\circ$ and for the case of constant and variable Γ-factor, respectively. The quantities are normalized to the value at $\theta_{\rm obs} = 0^\circ$ as we are interested to consider relative rather than absolute variations. For the first case, we choose $\Gamma = 100$, while for the second case the chosen parameters are $\Gamma_{\rm max} = 100$, $\Gamma_{\rm min} = 1.1$, and $p = 1$ (see equation 20).

Let us first discuss the case of Γ-constant: for $\theta_{\rm obs} \leq \theta_{\rm jet}$, $E_{\rm p}$, and remains constant, while the pulse-average flux simply rescales with $t_{\rm p}$, as defined in equations (11) and (12). This is easily understood in view of the considerations made in previous section when $\theta_{\rm jet} > 1/\Gamma$ – the strong beaming effect suppresses any dependence of the spectral shape on $\theta_{\rm obs}$. On the other hand, when $\theta_{\rm obs} > \theta_{\rm jet}$, the strong boosting of the photons along the direction of motion, without any light-of-sight intercepting the jet top-hat, causes a strong drop in the observed flux, which progressively decreases as $\theta_{\rm obs}$ increases. The

Downloaded from https://academic.oup.com/mnras/article/501/4/5723/6067371 by universita di catania fac giurisprudenza emeroteca user on 13 December 2023

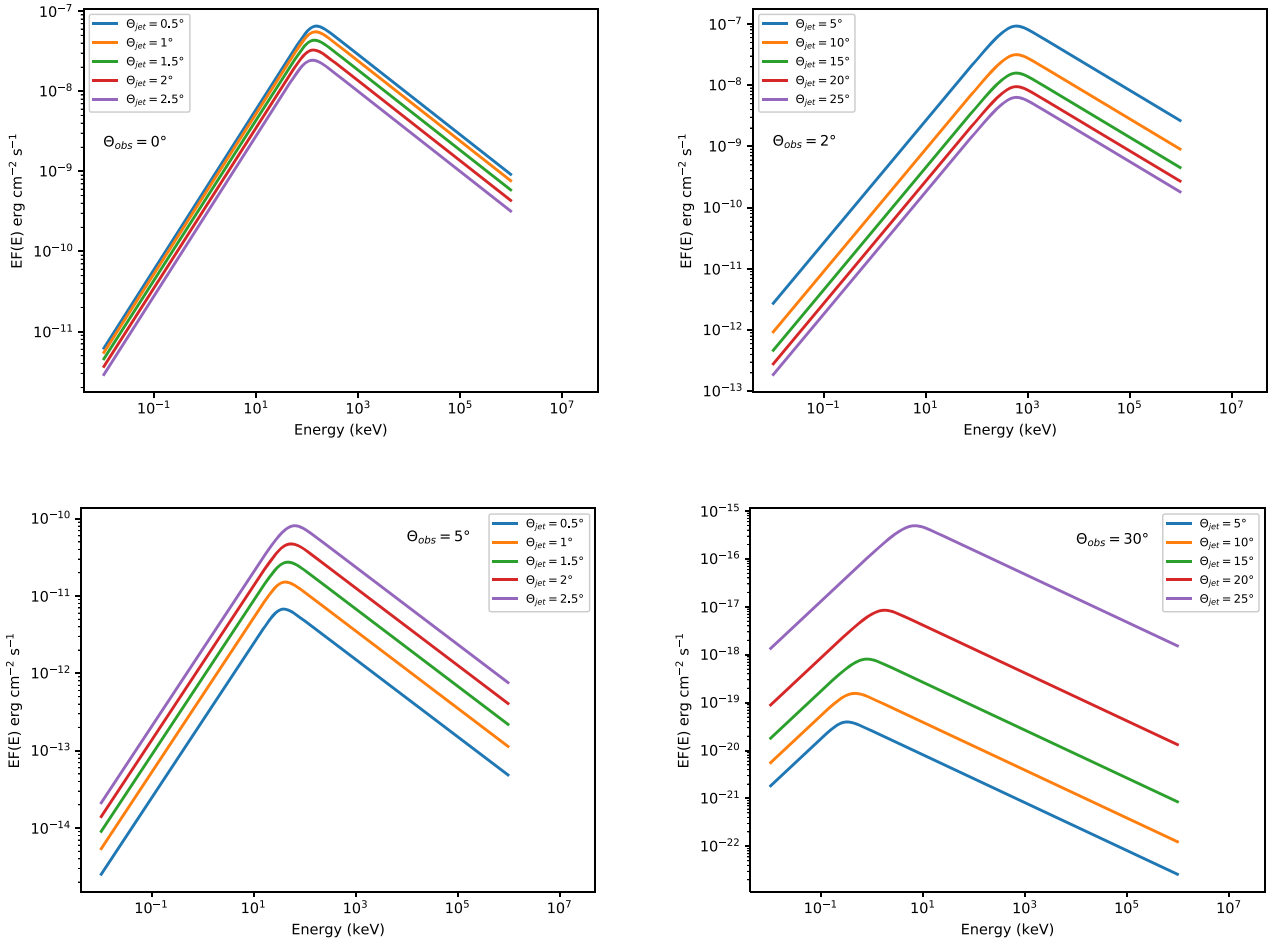

Figure 4. Simulated spectra for different values of the jet opening angle $\theta_{\rm jet}$. Top panels: on-axis case with $\Gamma = 20$ such that $\theta_{\rm jet} < 1/\Gamma$ (left) and $\Gamma = 100$ with $\theta_{\rm jet} > > 1/\Gamma$ (right). Bottom panels: off-axis case. The jet radius is 10^{12} cm, while the parameters of the comoving-frame SBPL emissivity law are the same of Fig. 3.

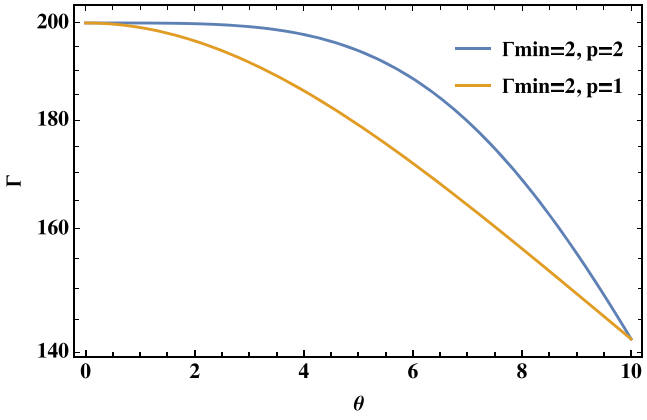

Figure 5. Dependence of the Γ-factor as a function of θ (see equation 20) with $\theta_{\rm jet} = 10^{\circ}$, $\Gamma_{\rm max} = 200$, $\Gamma_{\rm min} = 2$, and two different values of p.

main contribution comes here from the bottom part of the jet surface, as previously outlined (see Fig. 2).

The result changes slightly when considering a variable Γ-factor: when $\theta_{\rm obs} \leq \theta_{\rm jet}$, both $E_{\rm p}$ and the flux are mostly dictated by the value $\Gamma(\theta_{\rm obs})$ which is lower than $\Gamma(0)$. At the observational level,

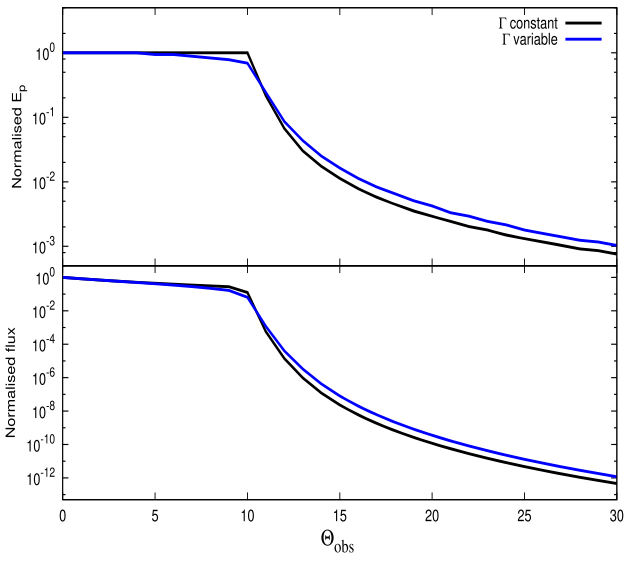

Figure 6. Dependence of the observed $E_{\rm p}$ and flux as a function of the observer viewing angle $\theta_{\rm obs}$ for a constant Lorentz factor $\Gamma = 100$ and for Γ obeying the law in equation (20) with $\Gamma_{\rm max} = 100$, $\Gamma_{\rm min} = 1.1$, and $p = 1$. We assumed $\theta_{\rm jet} = 10^{\circ}$, and the values are normalized to the case $\theta_{\rm obs} = 0^{\circ}$.

Downloaded from https://academic.oup.com/mnras/article/501/4/5723/6067371 by universita di catania fac giurisprudenza emeroteca user on 13 December 2023

however, a structured jet viewed at an angle θ_{obs} is indistinguishable from a Γ-constant jet with $\Gamma = \Gamma(\theta_{obs})$. On the contrary, when $\theta_{obs} > \theta_{jet}$ both E_p and the flux are higher than the case of constant Γ, because at the jet border from which most of the emission comes the Γ-factor achieves its minimum, and the Doppler boosting out of the direction towards the observer is less pronounced.

The situation may be of course different in the more complicated scenario of a structured jet as reported e.g. in Zhang et al. (2003), with a surrounding sub-relativistic cocoon, but this effect that results from magneto-hydrodynamical situations cannot be taken into account by our model.

In the version released for the XSPEC package we did not implement the dependence of Γ on the polar angle, to avoid having a too-high number of degrees of freedoms (additional Γ_{min} and p, see equation 20), which actually overcomes the number of observational spectral parameters.

4 THE E_P–E_{ISO} RELATION FOR ON-AXIS AND OFF-AXIS EVENTS

The main parameter driving the observed spectral peak energies and fluxes in relativistic outflows is the Γ-factor of the emitting material (Dermer 2004). We investigated this effect with a series of simulations at different Γ-values (not depending on θ), assuming the same SBPL spectrum in the comoving-frame with $E_0 = 10$ keV, $p_1 = 0$, $p_2 = 1.5$, and $\delta = 0.2$ (equation 16) and for a jet radius $R_{jet} = 10^{12}$ cm. The results are presented in Fig. 7.

We obtain a clear dichotomy between the on-axis and off-axis cases; when $\theta_{obs} \leq \theta_{jet}$ both E^i_p and L_{iso} increases as Γ does. In particular, for $\Gamma \gtrsim 20$ we obtain $E^i_p \propto \Gamma$ and $L_{iso} \propto \Gamma^2$, which in turn leads to the relation $E^i_p \propto L^{1/2}_{iso}$. On the contrary, when $\theta_{obs} > \theta_{jet}$ the two observable parameters progressively increase for moderate values of Γ up to $\sim$40, above which a decreasing power law-like behaviour occurs with $E^i_p \propto \Gamma^{-1}$ and $L_{iso} \propto \Gamma^{-4}$ – consequently, one obtains $E^i_p \propto L^{1/4}_{iso}$.

As a next step, we moved to the E^i_p–E_{iso} plane in order to reproduce the AR with a possibly *qualitative* representation of its intrinsic dispersion, which is known to have a variance higher than that coming from statistical uncertainties (Amati et al. 2002; Amati 2006). The data dispersion of the AR indicates that one or more physical and/or geometrical parameters play a role in addition to Γ which is claimed to have the leading role in dictating the observed slope $E^i_p \propto E^{0.5}_{iso}$.

Further considerations to point out for on-axis events are the following:

(i) E^i_p values (Y-axis) are $\propto E_0\ \Gamma$.
(ii) E_{iso} values (X-axis) are $\propto E_0\ K\ \Gamma^2\ R^2_{jet}$.

Moreover, all the parameters must be combined in order to reproduce not only the observed E^i_p–E_{iso} slope, but also the normalization which is of order of $\sim$100 (Amati, Frontera & Guidorzi 2009).

For off-axis events, E^i_p and E_{iso} have the same dependence on E_0, K, and R_{jet}, but with an inverse proportionality on Γ as shown above.

Based on the above considerations and constraints, we proceeded in the following way: let us define $G(P) = N(P_c, \sigma_P)$ as the normal Gaussian distribution of a given parameter P with P_c and σ_P its mean and standard deviation, respectively.

Performing simulations, we assumed $G(\Gamma) = N(100, 50)$ as derived from observational estimations (e.g. Ghirlanda et al. 2012). Sampling Γ-values from such a distribution poses constraints about the allowed range of E_0-values when comparing numerical results to observed values of E^i_p which cluster, a-part from a couple of cases below 10 keV, in a range of values from few tens keV to few MeV (Amati et al. 2009). With the assumed distribution of Γ, we found that a good choice for the comoving-frame break energy is $G(E_0) = N(5, 2)$.

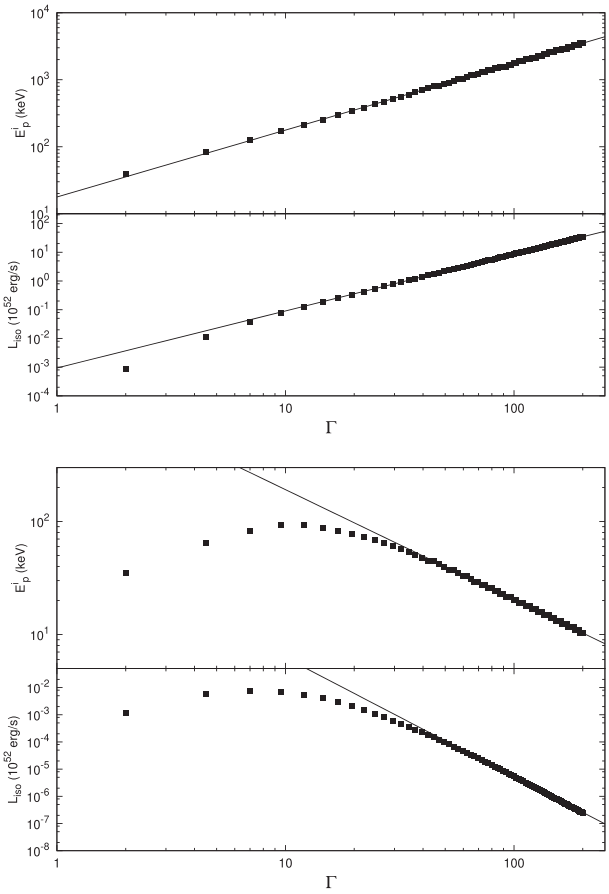

Figure 7. Behaviour of E^i_p and L_{iso} as a function of the Lorentz factor Γ, for the two cases of jet viewed on-axis (top panels) and off-axis (bottom panels). Jet parameters are $\theta_{jet} = 10^\circ$ and $R_{jet} = 10^{12}$ cm, while observer viewing angles are $\theta_{obs} = 5^\circ$ and $\theta_{obs} = 15^\circ$. Overplotted to data are the best-fitting power-law functions for $\Gamma \gtrsim 20$. For the on-axis case, the slopes are $E^i_p \propto \Gamma$ and $L_{iso} \propto \Gamma^2$, for the off-axis case $E^i_p \propto \Gamma^{-1}$ and $L_{iso} \propto \Gamma^{-4}$.

For the low-energy and high-energy index of the comoving-frame SBPL, we draw random values from two distributions with $G(p_1) = N(0, 0.5)$ and $G(p_2) = N(1.5, 0.5)$, respectively (see Nava et al. 2011, for a sample of best-fitting parameters using data from *BATSE* and *Fermi/GBM* sample).

The value of the jet half-opening angle θ_{jet} is instead drawn from a uniform distribution in the range $5^\circ - 20^\circ$, while the observer's viewing angle is sampled from a uniform distribution over $\cos(\theta_{obs})$ with $0 \leq \theta_{obs} \leq \theta_{jet}$ for on-axis events, $\theta_{jet} < \theta_{obs} < \theta_{jet} + 20^\circ$ in the other case. Finally, for the product of jet radius and SBPL normalization in such a way that $G(R^2_{12}/K_{20}) = N(150, 10)$, where R_{12} and K_{20} are in units of 10^{12} cm and 10^{20} ergs cm^{-2} s^{-1} keV^{-2} ster^{-1}, respectively.

It is worth pointing that the independent sampling of all parameters implies a diagonal covariance matrix which leads in turn to a variance of the data dispersion higher than that expected if at least some physical quantities are correlated. However, we are here interested in testing the E^i_p–E_{iso} main trend rather than its

Downloaded from https://academic.oup.com/mnras/article/501/4/5723/6067371 by universita di catania fac giurisprudenza emeroteca user on 13 December 2023

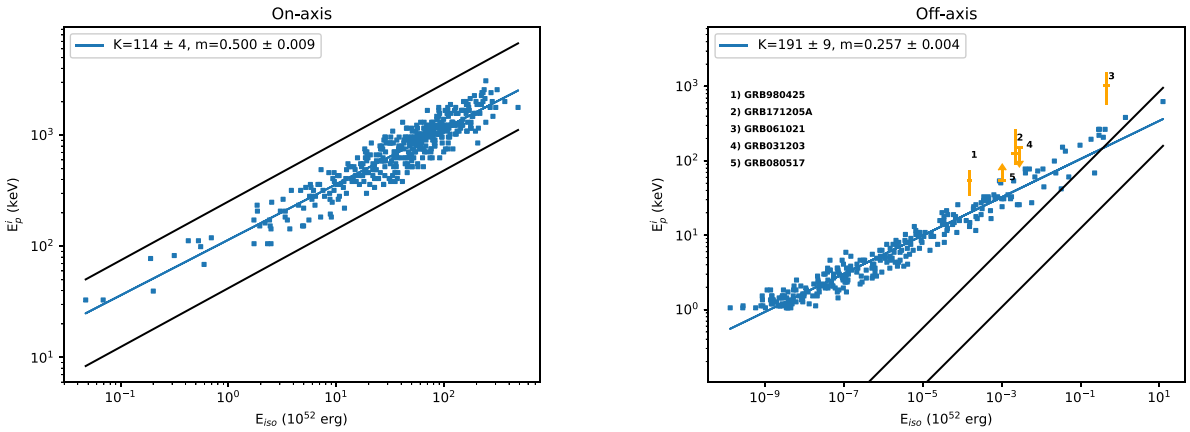

Figure 8. Simulated $E_{\rm p}^{\rm i}$–$E_{\rm iso}$ relation for events observed on-axis (left-hand panel) and off-axis (right-hand panel). References for true GRBs data are reported in Section 4. For GRB031203 and GRB080517, the upper and lower limits on $E_{\rm p}^{\rm i}$, respectively, are reported. The two continuous black lines correspond to the $\pm 2\sigma$ dispersion region of the observed $E_{\rm p}^{\rm i}$–$E_{\rm iso}$ relation reported by Amati et al. (2008).

intrinsic dispersion, and the random parameter sampling has been adopted just to simulate a *qualitative* representation of the data dispersion.

The results are reported in Fig. 8: as expected from the behaviour of $E_{\rm p}^{\rm i}$ and $L_{\rm iso}$ as a function of Γ (see Fig. 7), we obtain two different slopes for the $E_{\rm p}^{\rm i}$–$E_{\rm iso}$ relation for the two cases. For on-axis events, the index is $\sim$0.5, and the dominant contribution to the data variance around the best-fitting straight here comes from the random sampling of the comoving-frame SBPL parameters as well as the product R_{12}^2/K_{20}. The jet half-opening angle and the observer viewing angle play instead no role (see Fig. 6) under the condition $\theta_{\rm jet} > 1/\Gamma$ which is always satisfied here. Similar results have been obtained also by considering a structured jet according to equation (20). In this case indeed, the net effect is to put an event observed at given angle $\theta_{\rm obs}$ in the same location of the $E_{\rm p}^{\rm i}$–$E_{\rm iso}$ plane of events with constant Γ viewed at any angle $\theta_{\rm obs} < \theta_{\rm jet}$ but with $\Gamma = \Gamma(\theta_{\rm obs})$ or $\Gamma = \Gamma(\theta_{\rm jet})$ for on-axis and off-axis case, respectively.

For events with $\theta_{\rm obs} > \theta_{\rm jet}$, we have also added data taken from the literature for a few well-known outliers of the AR, namely GRB980425 ($z = 0.008$, Amati 2006), GRB 171205A/SN2017iuk ($z = 0.037$, D'Elia et al. 2018), GRB061021 ($z = 0.3463$, Nava et al. 2012), GRB031203 ($z = 0.106$, Martone et al. 2017), and GRB080517 ($z = 0.09$, Stanway et al. 2015).

We find that their position in the $E_{\rm p}^{\rm i}$–$E_{\rm iso}$ plane is more consistent with the theoretical one derived for off-axis sources, and for which the slope is $E_{\rm p}^{\rm i} \propto E_{\rm iso}^{0.25}$. This result strengthens the claim that the outliers of the AR are likely not intrinsically sub-luminous GRBs, but simply off-axis events which could be detected because of their nearness (Ramirez-Ruiz et al. 2005; Ghisellini et al. 2006). The simple geometric argument has additionally the advantage of avoiding to search for other unknown physical properties at the origin of the observable quantities. Our simulations endorse the interpretation that the AR relation arises from the observation of on-axis, highly relativistic jets and originates from relativistic kinematics effects of sources with given distribution of the Lorentz Γ-factor, the latter playing the role of leading parameter. On the other hand, the AR observed dispersion is due to intrinsic dispersion of GRB properties such as the comoving-frame spectral emissivity shape and the typical radius $R_{\rm jet}$ where the bulk of observed radiation during the prompt phase is released. For off-axis events, a correlation in the $E_{\rm p}^{\rm i}$–$E_{\rm iso}$ plane is still expected, but with a different slope ($\sim$0.25) whose value is closer to 1/3 such as for the cannonball model under the same off-axis assumption (Dado & Dar 2019).

It is also worth noticing that for both on-axis and off-axis sources, the assumption of a Gaussian distribution of the Γ-factors (if E_0 has a narrow distribution as well) leads to a clustering of points in the top-right and bottom-left part of the $E_{\rm p}^{\rm i}$–$E_{\rm iso}$ diagram, respectively. This is actually observed in the true data (e.g. Amati et al. 2008) and we claim that this is not due to observational bias effects, but arises from the intrinsic properties of the GRB population.

5 DISCUSSION

Despite the huge amount of theoretical work done until now to describe the spectral emission of the GRB prompt phase, the scientific community still uses phenomenological models for the X-ray spectral fitting. As mentioned earlier, GRBCOMP was the first physical model released for the XSPEC package. The model is based on hydrodynamical simulations performed by Chardonnet, Chechetkin & Titarchuk (2010) who investigated the SN formation due to pair-instability in very massive stars ($M \gtrsim 200\,{\rm M}_\odot$), a phenomenon that has received observational evidence (Gal-Yam & Leonard 2009; Gal-Yam et al. 2009).

The bulk of the emission in GRBCOMP is due to Comptonization of blackbody-like seed photons ($kT_{\rm bb} \sim$ few keV) by a Maxwellian population of hot electrons ($kT_{\rm e} \sim 100$ keV) moving outward the stellar surface at sub-relativistic speed. However, an association between pair-instability SN and GRBs still lacks, and GRBCOMP, albeit successful in fitting data and providing results consistent with simulations, appears strongly dependent on the GRB progenitor class, besides the fact of working out of the relativistic paradigm.

To overcome the phenomenological approach in the spectral analysis and work within the well-consolidated relativistic framework, we developed a numerical model that assumes emission from a top-hat jet using the single-pulse approximation (Yamazaki et al. 2003). Note that if the relativistic outflow is viewed on-axis ($\theta_{\rm obs} < \theta_{\rm jet}$), the observer can see only the top-hat surface and there is essentially no difference between a cone-like geometry extended over the radial distance from the centre of the system, and a geometrically thin shell.

We now briefly discuss the reliability of the best-fitting parameters while using the model for X-ray spectral analysis. First, let us define $F_{\rm CR}(E_{\rm obs}, \vec{P}_0, t)$ as the observed single-pulse light curve due

Downloaded from https://academic.oup.com/mnras/article/501/4/5723/6067371 by universita di catania fac giurisprudenza emeroteca user on 13 December 2023

to curvature radiation at some energy $E_{\rm obs}$, and for a given set of parameters $\vec{P}_0$. It is possible to reformulate equation (13) as

$$F_{\rm CR}(E_{\rm obs}, \vec{P}_0) = \frac{1}{t_{\rm spa}} \int_0^{t_{\rm spa}} F_{\rm CR}(E_{\rm obs}, \vec{P}_0, t){\rm d}t, \quad (21)$$

where $t_{\rm spa}$ is the single-pulse duration in the observer frame defined in equations (11) and (12).

On the other hand, the time-average spectrum over a general observed interval $t_{\rm grb}$ can be written as

$$F(E_{\rm obs}) = \frac{1}{t_{\rm grb}} \int_0^{t_{\rm grb}} F[E_{\rm obs}, \vec{P}(t), t]{\rm d}t, \quad (22)$$

where now $F[E_{\rm obs}, \vec{P}(t), t]$ is the true source light curve and $\vec{P}(t)$ is the time-dependent array of parameters describing the spectrum. The SPA model best-fitting parameters are thus the ones which minimize the difference between the right-hand terms in equations (21) and (22). In this context, the array $\vec{P}_0$ is a proxy of $< \vec{P}(t) >$, where the latter quantity is to be intended as averaged over $t_{\rm grb}$.

In a subsequent paper, we will present detailed time-dependent results in the framework of SPA for on-axis and off-axis events, together with mathematical tools for reproducing light curves as compliant as possible with observations.

Despite the above-described approximation, we outline how the proposed model is able to naturally reproduce the observed $E^{\rm i}_{\rm p}$–$E_{\rm iso}$ relation (AR) for on-axis events, at the same time providing a straightforward explanation for the outliers in terms of simple viewing angle effects. This results strengthen the idea that the main characteristics of the sources are caught from the observational point of view, allowing to consider with good confidence the physical and/or geometrical parameters inferred from the spectral fitting procedure.

For pratical purposes, it is also important to point out that for $\theta_{\rm obs} < \theta_{\rm jet}$ the observed peak energy $E_{\rm p}$ and the flux are essentially independent on $\theta_{\rm obs}$ (see Fig. 6), and this allows to reduce the space parameter dimension by one degree of freedom by setting $\theta_{\rm obs}$ to any value from 0 to $\theta_{\rm jet}$ in the X-ray spectral fitting procedure for all GRBs obeying the AR, i.e. are seen on-axis. The latest condition can be preliminarly tested by performing spectral fitting with e.g. the usual Band function (Band et al. 1993) and checking the position of the GRB in the $E^{\rm i}_{\rm p}$–$E_{\rm iso}$ plane. Moreover, under the same on-axis condition, most of the contribution to the flux comes from a region of width $\theta \sim 1/\Gamma$ centred along the direction to the observer (see Fig. 2), which is independent of the jet opening angle as long as $\theta_{\rm jet} \gtrsim 1/\Gamma$. This allows to further keep $\theta_{\rm jet}$ frozen to reasonable values (let say $10^\circ - 20^\circ$) during the fit, further lowering the number of free parameters. Some degree of degeneracy is instead expected between the comoving-frame break energy E_0 (see equation 16) and the Γ-factor as $E_{\rm p} \propto E_0\Gamma$ and $L_{\rm iso} \propto E_0\Gamma^2$. In this case, one should try to leave free both parameters and evaluate the magnitude of errors of the best-fitting values or keep free one of the two quantities from other independent evaluations.

Another point that deserves to be outlined is that the comoving-frame emissivity and the jet Γ-factor are here treated as potentially independent parameters. Actually, for the internal shock model particle acceleration as well as magnetic field values of the emission zone depend on the hydrodynamical conditions of the shocks forming between colliding shells. These in turn depend on the relative shell velocities and densities (e.g. Daigne & Mochkovitch 1998; Bošnjak, Daigne & Dubus 2009). The spectral shape and normalization in the comoving frame are related to the final Γ-factor of each couple of merged shells. It is however very difficult to provide within the context of a model for spectral fitting some analytical or numerical dependencies of the comoving-frame emissivity parameters on the Γ-factor. This would indeed require a different approach to the problem, with a set of coupled radiative transfer and hydrodynamical simulations from which eventually deriving explicit correlations to be tabulated and later imported into a model which, we outline again, needs to achieve a trade-off between computational speed and complexity. At the observational level, correlations between the jet Γ-factor and local emissivity need to be derived downstream from the model best-fitting parameters.

The presented model, albeit focused on the GRBs, can be considered *general*, having no limitations in the relativistic outflow Γ-values. A possible drawback is given by the fact that the emission from the lateral walls of a jet is neglected; this assumption is expected to essentially have little or no effect for $\theta_{\rm obs} \leq \theta_{\rm jet}$, while for off-axis events (if detectable) the fluxes computed from the model should provide a lower limit to the actual values, in particular for jets surrounded by a sub-relativistic cocoon (Kathirgamaraju et al. 2018). This would require however calculations of the emissivity profile across the jet radial direction, with definition of a $\Gamma(R)$-law, which is outside the scope of this work. Note however that emission from the lateral walls may be important for a jet having an appreciable radial extension, while for geometrical thin configurations with $\Delta R/R << 1$ (i.e. a shell) the top-hat emission here adopted provides a sufficiently good approximation.

6 CONCLUSIONS

The main purpose of our work was to make available for the XSPEC package the first relativistic non-phenomenological model for fitting the spectra of GRBs during the prompt phase. We thus developed a model for reproducing the observed spectra arising from the emission of a top-hat relativistic jet or a geometrically thin shell using the single pulse approximation. Despite unavoidable simplifications, necessary to have reasonable computational times with the XSPEC package, we have shown that the model reproduces the observed slope $\sim$0.5 in the plane $E^{\rm i}_{\rm p}$–$L_{\rm iso}$ or $E^{\rm i}_{\rm p}$–$E_{\rm iso}$ (AR) for on-axis events ($\theta_{\rm obs} < \theta_{\rm jet}$), and this effect naturally arises from pure relativistic kinematic effects, no-matter on the emissivity law in the comoving frame, provided a peak energy is of course present in the EF(E) spectrum. For off-axis events ($\theta_{\rm obs} > \theta_{\rm jet}$) the slope is instead $\sim$0.25. Many efforts have been made over years for explaining the physical origin of the AR (e.g. Guida et al. 2008; Dermer & Menon 2009; Ghirlanda et al. 2012; Titarchuk et al. 2012; Vyas, Pe'er & Eichler 2020) as well as its outliers, and in this work the disentangling between two distinct classes of observed events, which depends on the observer viewing angle, has been achieved with a thorough mathematical and numerical treatment.

We outline that the observational testing of this theoretical prediction can be also a very important scientific goal for the next generation of GRB observatories such as THESEUS (Amati et al. 2018), whose great enhanced sensitivity is expected to be able to catch a large sample of weak off-axis with enough statistics to allow time-resolved spectral analysis.

ACKNOWLEDGEMENTS

This project has received funding from the European Union's Horizon 2020 research and innovation program under the Marie Skłodowska-Curie grant agreement n. 664931 (RB).

Downloaded from https://academic.oup.com/mnras/article/501/4/5723/6067371 by universita di catania fac giurisprudenza emeroteca user on 13 December 2023

DATA AVAILABILITY

The source code of the model, labelled GRBJET, is available at the website address https://heasarc.gsfc.nasa.gov/xanadu/xspec/newmodels.html.

REFERENCES

Abbott B. P. et al., 2017a, ApJ, 848, L12
Abbott B. P. et al., 2017b, ApJ, 848, L13
Ahlgren B., Larsson J., Ahlberg E., Lundman C., Ryde F., Pe'er A., 2019, MNRAS, 485, 474
Aloy M. A., Müller E., Ibáñez J. M., Martí J. M., MacFadyen A., 2000, ApJ, 531, L119
Amati L., 2006, MNRAS, 372, 233
Amati L. et al., 2002, A&A, 390, 81
Amati L., Della Valle M., Frontera F., Malesani D., Guidorzi C., Montanari E., Pian E., 2007, A&A, 463, 913
Amati L., Guidorzi C., Frontera F., Della Valle M., Finelli F., Landi R., Montanari E., 2008, MNRAS, 391, 577
Amati L., Frontera F., Guidorzi C., 2009, A&A, 508, 173
Amati L. et al., 2018, Adv. Space Res., 62, 191
Arnaud K. A., 1996, in Jacoby G. H., Barnes J., eds, ASP Conf. Ser. Vol. 101, Astronomical Data Analysis Software and Systems V. Astron. Soc. Pac., San Francisco, p. 17
Band D. et al., 1993, ApJ, 413, 281
Barniol Duran R., Bošnjak Ž., Kumar P., 2012, MNRAS, 424, 3192
Basak R., Rao A. R., 2015, ApJ, 812, 156
Bégué D., Pe'er A., 2015, ApJ, 802, 134
Beloborodov A. M., 2011, ApJ, 737, 68
Beniamini P., Nakar E., 2019, MNRAS, 482, 5430
Berger E. et al., 2003, Nature, 426, 154
Bošnjak Ž., Daigne F., Dubus G., 2009, A&A, 498, 677
Burgess J. M., Bégué D., Greiner J., Giannios D., Bacelj A., Berlato F., 2019, Nat. Astron., 471
Campana S. et al., 2006, Nature, 442, 1008
Chardonnet P., Chechetkin V., Titarchuk L., 2010, Ap&SS, 325, 153
Crider A. et al., 1997, ApJ, 479, L39
Dado S., Dar A., 2019, ApJ, 884, L44
Daigne F., Mochkovitch R., 1998, MNRAS, 296, 275
D'Elia V. et al., 2018, A&A, 619, A66
Dermer C. D., 2004, ApJ, 614, 284
Dermer C. D., Menon G., 2009, High Energy Radiation from Black Holes: Gamma Rays, Cosmic Rays, and Neutrinos, Princeton University Press, Princeton and Oxford
Dermer C. D., Chiang J., Mitman K. E., 2000, ApJ, 537, 785
Eichler D., Livio M., Piran T., Schramm D. N., 1989, Nature, 340, 126
Fong W. et al., 2016, ApJ, 833, 151
Frontera F., Amati L., Farinelli R., Dichiara S., Guidorzi C., Landi R., Titarchuk L., 2013, ApJ, 779, 175
Fynbo J. P. U. et al., 2004, ApJ, 609, 962
Gal-Yam A., Leonard D. C., 2009, Nature, 458, 865
Gal-Yam A. et al., 2009, Nature, 462, 624
Gehrels N. et al., 2004, ApJ, 611, 1005
Ghirlanda G., Nava L., Ghisellini G., Celotti A., Burlon D., Covino S., Melandri A., 2012, MNRAS, 420, 483
Ghisellini G., Lazzati D., 1999, MNRAS, 309, L7
Ghisellini G., Ghirlanda G., Mereghetti S., Bosnjak Z., Tavecchio F., Firmani C., 2006, MNRAS, 372, 1699
Guida R., Bernardini M. G., Bianco C. L., Caito L., Dainotti M. G., Ruffini R., 2008, A&A, 487, L37
Guidorzi C. et al., 2009, A&A, 499, 439
Heussaff V., Atteia J. L., Zolnierowski Y., 2013, A&A, 557, A100
Kaneko Y., Preece R. D., Briggs M. S., Paciesas W. S., Meegan C. A., Band D. L., 2006, ApJS, 166, 298
Kathirgamaraju A., Barniol Duran R., Giannios D., 2018, MNRAS, 473, L121
Katz J. I., 1994, ApJ, 432, L107
Lazzati D., Ghisellini G., Celotti A., Rees M. J., 2000, ApJ, 529, L17
Liang E., Zhang B., Virgili F., Dai Z. G., 2007, ApJ, 662, 1111
Li L.-X., Paczyński B., 1998, ApJ, 507, L59
Lundman C., Pe'er A., Ryde F., 2013, MNRAS, 428, 2430
Margutti R. et al., 2017, ApJ, 848, L20
Martone R., Izzo L., Della Valle M., Amati L., Longo G., Götz D., 2017, A&A, 608, A52
Mészáros P., 2006, Rep. Prog. Phys., 69, 2259
Meszaros P., Rees M. J., 1993, ApJ, 405, 278
Mészáros P., Rees M. J., 2001, ApJ, 556, L37
Meszaros P., Rees M. J., Papathanassiou H., 1994, ApJ, 432, 181
Mizuta A., Nagataki S., Aoi J., 2011, ApJ, 732, 26
Morsony B. J., Lazzati D., Begelman M. C., 2007, ApJ, 665, 569
Nakar E., Ando S., Sari R., 2009, ApJ, 703, 675
Nava L., Ghirlanda G., Ghisellini G., Celotti A., 2011, MNRAS, 415, 3153
Nava L. et al., 2012, MNRAS, 421, 1256
Pian E. et al., 2006, Nature, 442, 1011
Preece R. D., Briggs M. S., Mallozzi R. S., Pendleton G. N., Paciesas W. S., Band D. L., 1998, ApJ, 506, L23
Proga D., MacFadyen A. I., Armitage P. J., Begelman M. C., 2003, ApJ, 599, L5
Ramirez-Ruiz E., Celotti A., Rees M. J., 2002, MNRAS, 337, 1349
Ramirez-Ruiz E., Granot J., Kouveliotou C., Woosley S. E., Patel S. K., Mazzali P. A., 2005, ApJ, 625, L91
Rhoads J. E., 1997, ApJ, 487, L1
Ryde F. et al., 2010, ApJ, 709, L172
Salafia O. S., Ghisellini G., Pescalli A., Ghirland a G., Nappo F., 2016, MNRAS, 461, 3607
Salafia O. S., Barbieri C., Ascenzi S., Toffano M., 2020, A&A, 636, A105
Sari R., Piran T., Halpern J. P., 1999, ApJ, 519, L17
Soderberg A. M. et al., 2004, Nature, 430, 648
Soderberg A. M. et al., 2006, Nature, 442, 1014
Stanway E. R., Levan A. J., Tanvir N., Wiersema K., van der Horst A., Mundell C. G., Guidorzi C., 2015, MNRAS, 446, 3911
Starling R. L. C. et al., 2011, MNRAS, 411, 2792
Titarchuk L., Farinelli R., Frontera F., Amati L., 2012, ApJ, 752, 116
Troja E. et al., 2018, Nat. Commun., 9, 4089
van Eerten H., Zhang W., MacFadyen A., 2010, ApJ, 722, 235
Vyas M. K., Pe'er A., Eichler D., 2020, ApJ, preprint (arXiv:2011.02973)
Woosley S. E., 1993, ApJ, 405, 273
Yamazaki R., Ioka K., Nakamura T., 2003, ApJ, 593, 941
Zhang W., Woosley S. E., MacFadyen A. I., 2003, ApJ, 586, 356
Zhang W., Woosley S. E., Heger A., 2004, ApJ, 608, 365
Zhang B. B. et al., 2018, Nat. Astron., 2, 69

This paper has been typeset from a TEX/LATEX file prepared by the author.

Downloaded from https://academic.oup.com/mnras/article/501/4/5723/6067371 by universita di catania fac giurisprudenza emeroteca user on 13 December 2023